Journal of Visualization, Vol. 9, No. 1 (2006)13-21

Vortex Flow Patterns of a Heaving Foil

Yang, C. J.*[1] and Lee, Y. H.*[2]

*1 Satellite Venture Business Laboratory, 1-1 Sensui-cho, Tobata-ku, Kitakyushu-shi, Fukuoka, 804-8550, Japan. E-mail: cjyang70@pivlab.net
*2 Division of Mechanical and Information Engineering, College of Engineering, Korea Maritime University, 1 Dongsam-dong Youngdo-ku, Busan, 606-791, Korea.

Received 17 November 2004
Revised 18 August 2005

Abstract : It is known that an oscillating foil can produce a thrust force through the generation of a reverse Kármán vortex street and this can be expected to be a new highly effective propulsion system. A heaving foil model was made and it was operated within a circulating water channel. The wake formation behind the heaving foil was visualized using PIV method and a dynamic thrust force was measured using a mini 6-axis force sensor based on force and moment detectors. We examined various conditions such as reduced frequency and amplitude in NACA 0010 profile. The vortical patterns in the wake were classified according to the wake mode and force data.

Keywords : Unsteady flow, Heaving foil, Strouhal Number, Dye Visualization, PIV, Reverse Kármán vortex street.

1. Introduction

The unsteady flow over oscillating foils has been studied by a number of investigators using theoretical and numerical techniques. The classical unsteady aerodynamic theory of oscillating foils was studied as a result of interest in aircraft flutter problems in inviscid incompressible flow (Theodorson, 1935). In particular, the problem regarding the phenomena of unsteady vortex dynamics has come to occupy an important position in bio-fluid-dynamics, i.e., insects, birds and fish (Lighthill, 1970). In recent years, several physical and mechanical designs, evolved in fish tails and insect wings, are currently inspiring robotic devices for propulsion and maneuvering purposes in vehicles such as UMV (Unmanned Underwater Vehicle), MEMS (Micro -Electro Mechanical Systems) and MAV (Micro Aerial Vehicle) (Ho and Tai, 1996).

It has been reported that a heaving foil can produce thrust through the peculiar flow formation known as a reverse Kármán vortex street from the trailing-edge (Lai and Platzer, 1999). This average flow is unstable with a narrow range of frequencies of amplification. The unsteady fluid mechanism is characterized by the formation of a strong vortex on the surface behind the foil. The interaction between the unsteady vortices shed by the foil and inherent dynamics of the unstable wake results in the formation of patterns of large-scale eddies. Moreover, the formation of vortices in the wake of the oscillating foil is closely associated with the propulsive efficiency (Anderson et al., 1998).

Meanwhile, some progress has been made by these studies in analyzing the characteristics of vortices, but the topological structure and its relationship to thrust generation in the near wake still remain obscure to us. Moreover, most of previous experimental approaches to these structures have

been made using visual observation and point measurements. In qualitative visualization, however, the presence of discrete vortices merely based on the rolling-up of the streaklines cannot be positively identified. Particle Image Velocimetry (PIV) therefore can be a powerful alternative to flow visualization techniques such as tuft, trace and optical-based schlieren method and the previous point-wise and time-mean velocity measurement such as LDV (Laser Doppler Velocimetry) and HWA (Hot Wire Anemometer) (Adrian, 1991).

To investigate the unsteady vortex dynamics, which is crucial to the force generation on the heaving foil, this experiment therefore was performed in a circulating water channel using the technique of two-color dye injection visualization and a spatio-temporal resolved PIV system based on cross correlation method at low Reynolds number region. As results, we showed that the heaving motion over a certain non-dimensional heaving velocity makes the reverse Kármán vortex street in the wake. The overall features of the unsteady vortex dynamics also have been investigated.

2. Experimental Procedure

Figure 1 shows the experimental apparatus. Experiments were conducted on a NACA 0010 foil with chord equal to 60 mm and span 200 mm, fitted with circular end plates to ensure two-dimensional flow and to reduce end effects. The flow generation system was a circulating water tunnel and main flow velocity was 0.067 m/s. The water channel had the following dimensions: 675 mm (H) × 200 mm (V) × 300 mm (D). A PTP (Point To Point) digitally controlled Ternary DC servo motor (RMJ0711-001, Dyadic systems) allowed for a sinusoidal motion with heaving frequency and amplitude arbitrarily. The motion was transmitted to the foil through universal joint and ball screw. The size of the analyzed region was 200 mm (H) × 100 mm (V).

The wake flow was visualized using coloring issued from two small injection tubes imbedded in the foil and was recorded on videotape by a Digital video camera (DCR-VX 1000, SONY) through a plane mirror installed under the water channel. A halogen sheet light (150 W, MHF-150L, MORITEX) was used for the 2-D plane illumination through a line light guide and lens. Uranine (Green) and Rohdamin B (yellow) were used as dyes. They naturally flowed out from the inlet tap on the foil by gravity.

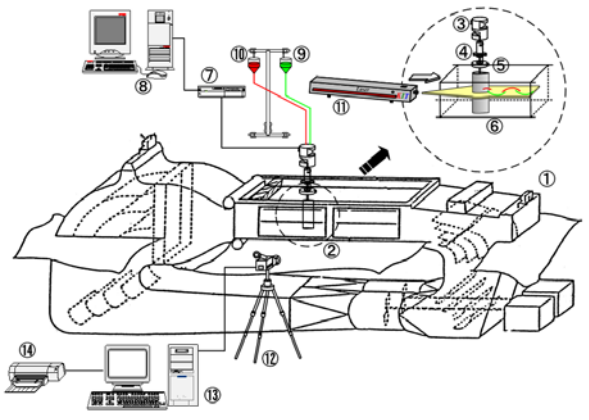

1. Water tunnel
2. Test section
3. DC servo motor
4. Ball screw
5. NACA 0010
6. 6-axis sensor
7. Motor driver
8. Motor controller
9. Uranine
10. Rohdamin B
11. Ar-ion Laser
12. High speed camera
13. Image processor
14. Printer

Fig. 1. Experimental apparatus.

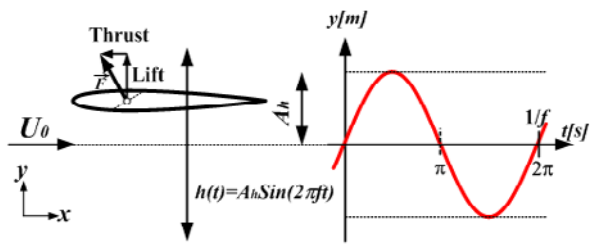

Fig. 2. Trajectory of the foil.

For illuminating the flow field of the PIV experiment, a 4 W water-cooled Argon-Ion laser with a fiber optic assembly generates a two-dimensional thin sheet light of about 2 mm thickness. Orgasol particles with mean diameter 50 μm and specific weight 1.1 g/cm^3 are seeded. The scattered light is captured by a high-speed camera (Phantom V5.0, Phantom) with a large internal memory block. This camera has an 8-bit sensor array of 1,024 × 1,024 pixels and can obtain images at a maximum speed of 1000 frames/sec with full resolution and 62,500 frames/sec with partial resolution (256 × 32 pixels). The large internal memory block (1,024 MB) allows 1,024 frames at full resolution to be saved successively. Phase difference between two images for cross correlation influences the accuracy of phase resolution. The smaller phase difference between two images becomes the more the accuracy of phase resolution increases. Maximum phase difference between two images for cross correlation was therefore set to under 2[pixel]. A spatio-temporal resolved PIV system, which can be achieved to increase the spatial resolution and dynamic range of detecting particle image displacements in PIV images, was adopted. As steps for the post processing, error removing, reallocation in grid and conversion of pixel to real unit procedures were performed. The divergence criterion satisfying the continuity equation was adopted in the error removal procedure. Error uncertainty by the automated procedure was on the average less than 2 % in the vector identification. In the present study, the phase detection is based upon the DC servo motor pulse signal and the streamwise velocity signal. And thus, the phase average was realized by taking an average over the conditional sampling at a given phase.

To investigate the unsteady fluid forces and associate them to visualization results, the forces acting on the heaving foil were measured. The unsteady fluid forces were measured with a mini 6-axis force sensor (MINI 2/10, BL AUTOTEC), placed at one end of the foil attachment, which is based on the principle of pressure pick-up device and characterized by simple structure and miniature size. A single heaving motion was imposed with various combinations of heaving frequency, f and amplitude, A_h. Figure 2 shows the trajectory of the heaving foil. The solid line is the heaving waveform ($h(t) = A_h Sin2\pi ft$). The non-dimensional frequency, called reduced frequency is defined as $k = 2\pi f(c/2)/U_0$ (conventionally half the chord is used), where U_0 denotes the free-stream velocity. The Strouhal number (non-dimensional heaving velocity) is defined as $St = f \cdot 2A_h/U_0$. Note that St measures the ratio of the heaving velocity and the mean forward velocity. Experiments were conducted with Strouhal numbers between 0.0 and 0.36, while an intense investigation was also made for the effect of a *neutral* wake structure, where a pair of vortices with different rotating velocity stood in a line.

3. Results and Discussion

3.1 Two-Color Dye Injection Visualization

Figure 3 shows wake patterns past the oscillating foil at a certain time in a shedding cycle. Dye visualizations were carried out at the Reynolds number, Re = 4.0×10^3. Here, heaving foil undergoes periodic motion and the flow is from left to right and V1 denotes vortices shed from the upper surface of the foil and V2 denotes vortices shed from the lower one. Figure 3(a) shows vortex pairs of counter-rotating vortices in the wake. This wake structure displays similar vortex arrangement of a Kármán vortex street observed in the wake behind bluff bodies. For $St < 0.03$, the wake does not roll up into discrete vortices and retains its wavy forms. In the case of Fig. 3(b), the small increase of Strouhal number places the shed vortices on the near wake centerline. Well-organized vortices are present, while two vortices (V1, V2) per cycle are shed into the wake. The alternating vortices are positioned in the direction of the wake centerline and indicate the typical *neutral* structure, which yields zero force when averaged over one period of oscillation as reported by von Kármán and Burgers (1935). Figure 3(c) shows the flow visualization at $St = 0.23$. Especially, a reversed flow pattern (V1, V2) is generated in comparison with Fig. 3(a). This structure is the very reverse Kármán vortex street, which has opposite circulation and different strength. Jones et al. (1998) and Yang et al.

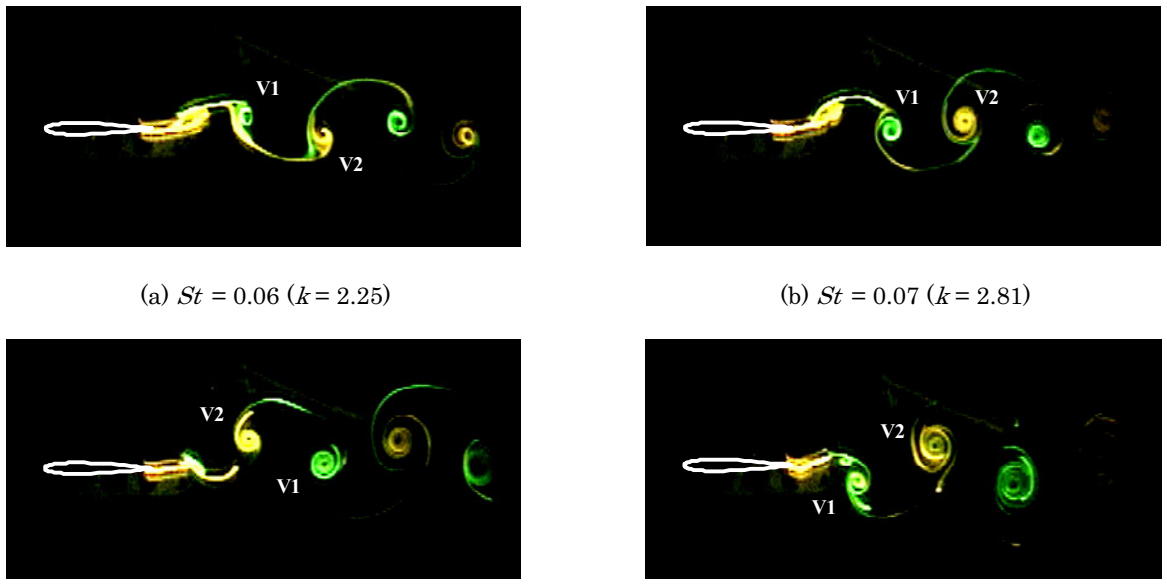

(a) St = 0.06 (k = 2.25) (b) St = 0.07 (k = 2.81)

(c) St = 0.23 (k = 4.22) (d) St = 0.30 (k = 5.63)

Fig. 3. Wake patterns behind the heaving foil (A_h/c = 0.04 in (a), (b) and A_h/c = 0.09 in (c), (d)).

(2002) have reported that the formation of the reverse Kármán vortex street is closely associated with the vortex structure of thrust production. When averaged over one period of oscillation, the wake has the form of a jet in flow structure, which shows the reverse Kármán wake accompanied by the interaction between vortices shed by the oscillating foil and innate dynamics of the wake. Moreover, it is shown that the vortices become to be large in magnitude as the non-dimensional frequency increases. For such cases the wake survey results will compare with vorticity contour plots and trajectories of vortex center in next section. Figure 3(d) shows the clearest vortex formation. It can be also seen that the spacing of the vortices in the wake decreases their prominence with progression of Strouhal number in same heaving amplitude.

3.2 Time-Mean Velocity Field

PIV measurements were also conducted at the Reynolds number, $Re = 4.0 \times 10^3$ as stated earlier. Figure 4(a) shows ensemble-averaged velocity field in the wake of the foil undergoing sinusoidal heave motion in amplitude, A_h/c = 0.04. To obtain the ensemble-averaged velocity field, 750 instantaneous velocity fields of consecutive images were averaged. Figure 4(b) shows streamlines from the ensemble-averaged velocity field. The distribution of streamlines from ensemble-averaged velocity field shows the symmetry of the flow field around the heaving foil. Thus, note that reversed-flow region and reattachment bubble which are founded in the wake past bluff bodies in shear-layer transition regime are not found in the case of the wake behind the oscillating foil. This can be explained by location and orientation of the wakes vortices, as illustrated in Fig. 3, for drag-indicative and thrust-indicative wakes.

Figure 5(a) shows mean streamwise velocity profiles. The mean velocity profiles were measured 1.25c downstream of the center of the foil in different Strouhal numbers. The variations during a cycle of oscillation were obtained by averaging long-time velocity data behind the heaving foil. The averaged wake profiles are different at each Strouhal numbers due to the changes in force and momentum integral around the foil. As Strouhal number increases ($St > 0.07$), it can be seen that the wake profile with velocity deficit can be transformed into the wake with velocity excess (jet). Because the mean velocity of the perturbation close to the wake centerline is advected downstream more quickly than the more off-centered parts in jet. LDV Result (NACA0012) by John et al. (1998)

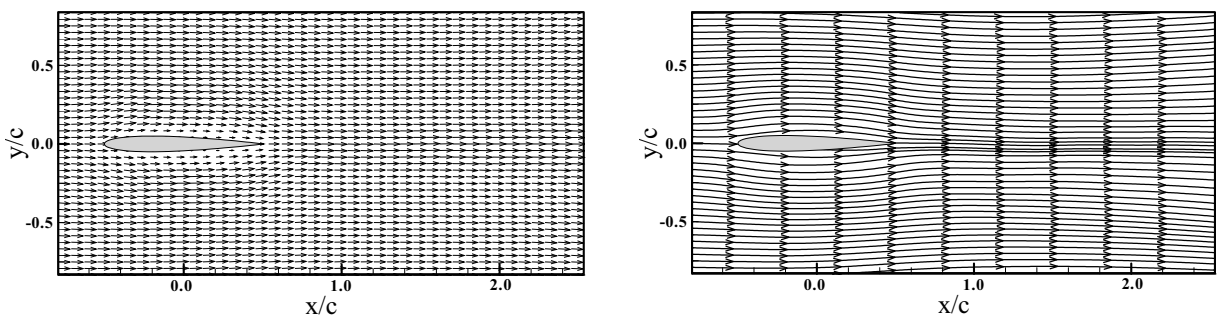

(a) Ensemble averaged velocity field (b) Streamlines from ensemble averaged velocity field

Fig. 4. Ensemble averaged velocity field and streamlines (k = 4.22, A_h/c = 0.04).

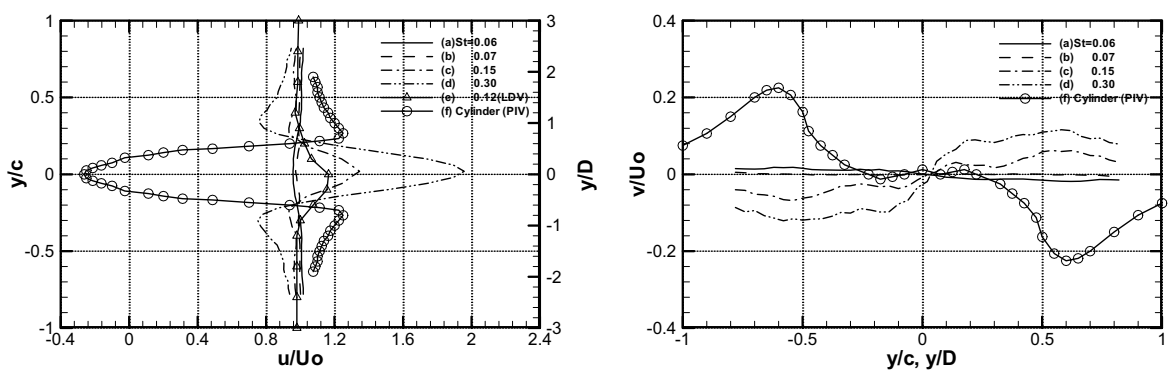

(a) Mean streamwise velocity profiles (b) Mean cross-stream velocity profiles

Fig. 5. Mean streamwise and cross-stream velocity profiles (x/c = 1.25).

also shows the jet velocity. On the contrary, PIV result in the wake of the circular cylinder (D: diameter) at Reynolds number, $Re = 3.9 \times 10^3$, shows the wake profile with velocity deficit and shows negative velocity region which means the reverse flow. Meanwhile, in the case of $St = 0.07$, the mean velocity profile shows that a condition exists that the wake has no velocity deficit and excess. This condition occurs when the alternating vortices are positioned on the nearly straight line as shown in Fig. 3(b). This will be discussed with trajectory of vortex center and the temporal evolution of the shedding vortices in Fig. 6. Figure 5(b) shows the mean cross-stream velocity profiles. As Strouhal number increases, it can be seen that the transverse wake profiles are rotated in a counter-clockwise direction, and then, the profiles switched signature in the longitudinal axis. The reason for this is switched vortex formation in the wake as shown in Fig. 3. Thus the mean v-component velocity is advected cross-stream adversely as Strouhal number increases ($St > 0.07$). On the other hand, the transverse wake profile of the circular cylinder showed somewhat constant pattern.

3.3 Vorticity and Trajectory of Vortex Center

Figure 6 shows contour plots of vorticity and trajectories of vortex center behind the heaving foil at different Strouhal numbers. We examined the quantitative features of the associated vortex dynamics in these four cases. To accurately estimate the vorticity defined in terms of the velocity gradient, an adaptive scheme coupled with a least squares second-order polynomial at different grid spaces was adopted to minimize the total error which is defined as the summation of the

experimental and truncation errors (Lourenco, 1995). The solid and dashed line contours mark the vorticity levels of the shedding vortex. The solid/dashed line contours correspond to ζ_z with maximum level $|\zeta_z|_{max} = 0.02$ s^{-1} and increment $|\zeta_z| = 0.004$ s^{-1}. In Fig. 6(a), the induced flow has a component moving backward with respect to the foil to generate the wake pattern like Kármán vortex street as seen in two-color dye-injection visualization. In the case of Fig. 6(b), a pair of vortices with different rotating velocity stood in a line as stated earlier. The vortex pattern showed no tendency to deviate from this alignment as it moves downstream. In Fig. 6(a), the trailing-edge vortex is relatively small and a weak leading-edge vorticity is bound in foil. And the size of the trailing-edge vortex in Fig. 6(b) is larger than that in Fig. 6(a), while leading-edge vorticity in still bound. In Fig. 6(c), an alternating vortex pattern is formed such that the vortex with positive circulation (counter-clock wise) is located on top half of the wake and the one with negative circulation in the lower half of the wake. Especially, the formation of a reverse Kármán vortex street is closely associated with magnitude of thrust production. Wang (2000) also reported that the optical frequency in flapping flight results from exploiting two intrinsic time scales, one governing the vortex growth, and the other governing the shedding of the vortex. Namely, high thrust was associated with the generation of moderately strong vortices, which subsequently combined with trailing-edge vorticity leading to the formation of a reverse Kármán vortex street as the non-dimensional frequency, called here in Strouhal number increases (> 0.08). Figure 6(d) shows that a very strong trailing-edge vortex forms and is shed well, while the wake consists of two vortices per cycle with development of the vorticity during the shedding process as will see in Fig. 7. A trend with increase of Strouhal number also is found the decrease in the wavelength of the vortices in the wake. But, increase of Strouhal number did not change the shape of the vortex structure in this region, only the size varied proportionate to the heaving frequency and amplitude.

In order to track trajectory in temporal evolution of the shedding vortices, we need to evaluate vortex center. Possible definitions of the vortex center are as follows: one is the peak position of the vorticity by evaluating complex eighenvalues of the velocity gradient tensor after conditional

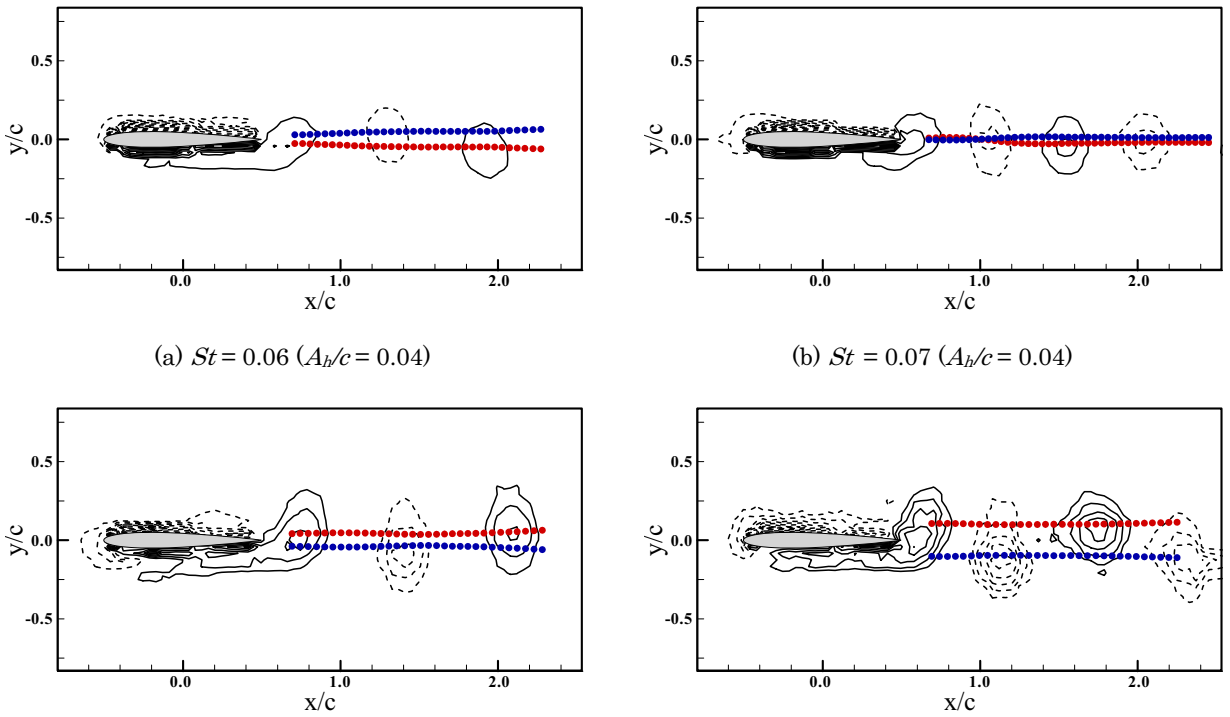

(a) $St = 0.06$ ($A_h/c = 0.04$) (b) $St = 0.07$ ($A_h/c = 0.04$)

(c) $St = 0.14$ ($A_h/c = 0.09$) (d) $St = 0.15$ ($A_h/c = 0.09$)

Fig. 6. Phase-averaged vorticity field in the *x*-*y* plane (All phases correspond to π).

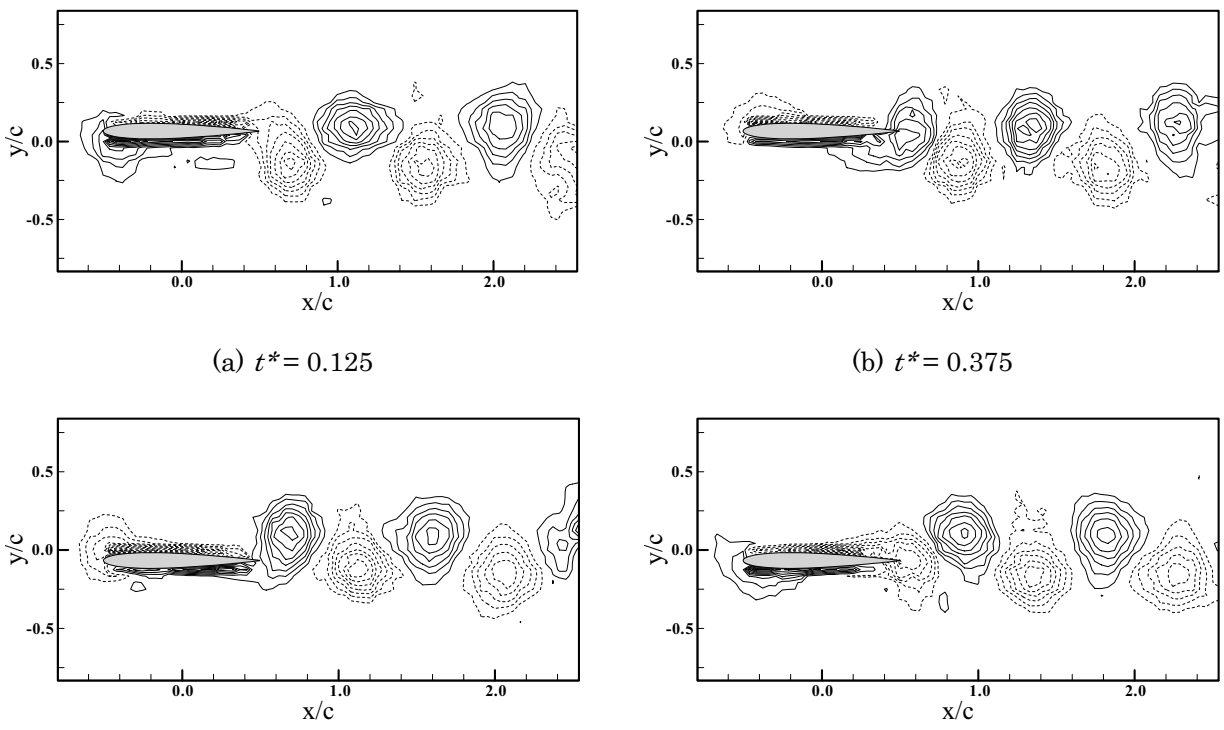

(a) t^*= 0.125 (b) t^*= 0.375

(c) t^*= 0.625 (d) t^*= 0.875

Fig. 7. Development of the vorticity during the shedding process (St = 0.15, t^* = t/($1/f$)).

averaging (Perry, 1987) and the other is the centroid of the vorticity field (Cantwell & Coles, 1983). The former is easy to realize but may result in high uncertainty. In the present study, the latter is adopted with the centroid evaluated in the x-y plane. Vortex center (x_c, y_c) is defined as

$$x_c = \frac{1}{\Gamma}\oint x\langle\zeta_z\rangle dl$$
$$y_c = \frac{1}{\Gamma}\oint y\langle\zeta_z\rangle dl \quad (1)$$

where Γ $(=\oint u(x,y)dl)$ denotes the circulation and dl denotes a section of a closed contour of integration. The summations in each case are allowed for values of $\zeta_z / |\zeta_z|_{\max} \geq 0.5$ to avoid relatively noisy data, where $|\zeta_z|_{\max}$ is the maximum vorticity in the wake region. The trajectory of vortex center is tracked by identifying the centroids of vorticity in the downstream region as stated before. Each symbol represents the position of the vortex center every 1/30 sec. Red dot symbols in Fig. 6, are acquired in down-stroke, and blue data in up-stroke is mirrored due to symmetry of the wake. The RMS error between the instantaneous and phase-averaged data identified based on the centriod of the vorticity field results to 1.3% for streamwise locations and 4.5% for cross-stream locations. Interestingly, apart from the separating shear layers to the oscillating foil, the trailing-edge vortex is moved upward in down-stroke and downward in up-stroke at the rear of the foil as Strouhal number increases. This is important because the shed vortices are switched in the wake and make the reverse Kármán vortex street.

Figure 7 shows the temporal evolution of the phase-averaged vorticity during the shedding process. The solid/dashed line contours correspond to ζ_z with maximum level $|\zeta_z|_{\max}$ = 0.02 s^{-1} and increment $|\zeta_z|$ = 0.002 s^{-1}. A strong trailing-edge vortex forms and is shed well just after the foil reaches the maximum amplitude excursion, while the wake consists of two vortices per cycle.

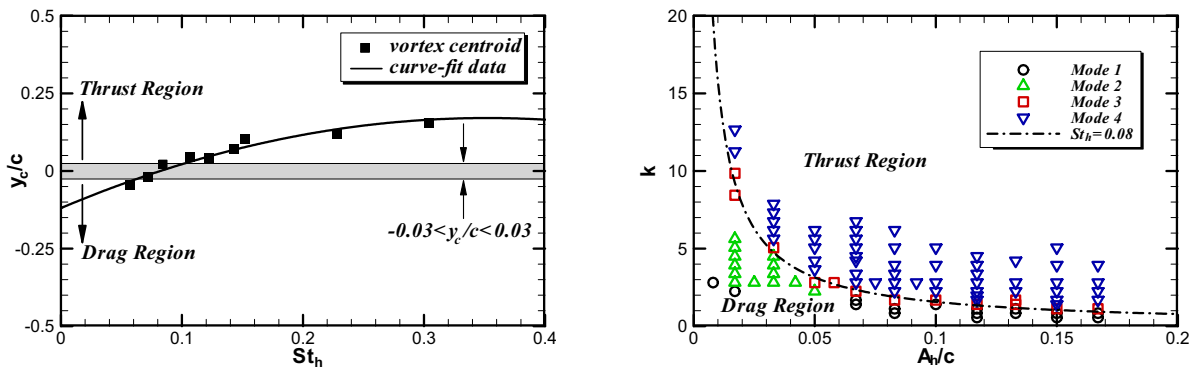

(a) Cross-stream locations of vortex center (b) Flow patterns behind the heaving foil

Fig. 8. Wake classification of the vortex patterns.

3.4 Wake Classification

Fig. 8 shows the cross-stream locations of the vortex center and wake classification at the vortex patterns behind the heaving foil. In Fig. 8(a), to classify the previous flow patterns, the distance (y_c) between the centerline of the flow field and a shed vortex center was measured in the near wake ($0.6 < x/c < 2.6$). And then, if *neutral flow pattern*, where neither drag nor thrust is generated as shown in Fig. 6(b), was limited to $|y_c/c| < 0.03$, it can be seen that it exists around $St = 0.08$.

Triantafyllou et al. (1993) and John et al. (1998) show a plot, classifying the experimental results based purely on visual observation of the unsteady vortex dynamics. More detailed wake classification of the force measurements and vortex patterns (modes) based on PIV data is shown in Fig. 8(b). Open circle (Mode 1) corresponds to wavy forms, which do not roll up into discrete vortices in the streamwise direction. Mode 2 indicates the Kármán vortex pattern as shown in Fig. 6(a), whereas Mode 4 does the revered Kármán vortex pattern as shown in Fig. 6(c) and (d). Mode 2 like Kármán vortex pattern showed at only low amplitude region. Mode 3 also showed that a condition existed at which the wake has no momentum deficit or excess as seen in mean velocity profiles and trajectory of the vortex center. Dotted line of constant Strouhal number (St = 0.08) is included, demonstrating the approximate dependence of the experimental data on the Strouhal number. Mode 4 showed over the dotted line. Furthermore, at above Mode 4, the vortex street deflected up or down is generated randomly due to flow disturbances and instabilities as John et al. (1998) showed.

4. Conclusion

Two-color dye injection visualization and PIV experiments were performed to investigate the vortex flow patterns of a heaving foil after parametric searches, which were added by a consideration of mechanisms governing the dynamics of its wake. The conclusions of the present study are enumerated in the following.

1) As Strouhal number is greater than 0.08, wake profile with velocity deficit can be transformed into the wake with velocity excess.
2) After evaluating vortex center, flow patterns in the wake investigated using tracking trajectories in temporal evaluation of the shedding vortices. Apart from the separating shear layers to the oscillating foil, the trailing-edge vortex is moved upward in down-stroke and downward in up-stroke at the rear of the foil as Strouhal number increases.
3) Wake classification of the vortex patterns based on quantitative data was obtained. And flow

visualizations showed that high thrust was associated with the generation of moderately strong vortices, which subsequently combined with trailing-edge vorticity leading to the formation of a reverse Kármán vortex street as Strouhal number increases.

References

Adrian, R. J., Particle-imaging techniques for experimental fluid mechanics, Annual Review Fluid Mechanics, 23 (1991), 261-304.
Anderson, J. M., Streitlien, K., Barrett, D. S. and Triantafyllou, M. S., Oscillating foils of high propulsive efficiency, Journal of Fluid Mechanics, 360 (1998), 41-72.
Cantwell, B. and Coles, D., An experimental study of entrainment and transport in the turbulent near wake of a circular cylinder, Journal of Fluid Mechanics, 136 (1983), 321-374.
Ho, C. M. and Tai, Y. C., MEMS and fluid flow, ASME Journal of Fluids Engineering, 30 (1996), 579-612.
Jones, K. D., Dohring, C. M. and Platzer M. F., Experimental and computational investigation of the Knoller-Bentz effect, AIAA Journal, 36-7 (1998), 1241-1246.
Lai, J. C. S. and Platzer, M. F., Jet characteristics of plunging foil, AIAA Journal, 37-12 (1999), 1529-1537.
Lighthill, M. J., Aquatic animal propulsion of high hydromechanical efficiency, Journal of Fluid Mechanics, 44 (1970), 265-301.
Lourenco, L. and Krothapalli, A., On the Accuracy of Velocity and Vorticity Measurements with PIV, Exp. Fluids, 18 (1995), 421-428.
Perry, A. E. and Chong, M. S., A Description of Eddying Motions and Flow Patterns Using Critical-Point Concepts, Ann. Rev. Fluid Mech., 19 (1987), 125-155.
Theodorson, T., General theory of aerodynamic instability and the mechanism of flutter, NACA Report, 496 (1935).
Triantafyllou, G. S., Triantafyllou, M. S. and Gopalkrishnan, R., Optical thrust development in oscillating foils application to fish propulsion, Journal of Fluids and Structures, 7 (1993), 205-224.
von Kármán, T. and Burgers, J. M., General Aerodynamic Theory Perfect Fluids, (1935), Berlin-Springer.
Wang, Z. J., Vortex shedding and frequency selection in flapping flight, Journal of Fluid Mechanics, 410 (2000), 323-341.
Yang, C. J., Tanaka, K. and Lee, Y. H., Vortex flow pattern of a flapping foil, 10th International Symposium of Flow Visualization (Kyoto, Japan), F0299 (2002-8).

Author Profile

Chang-Jo Yang: He received his B. Eng. and M. Eng. degrees in marine systems engineering from Korea Maritime University in 1993 and 1999. He also received his Dr. Eng. degree in 2003 from Kyushu Institute of Technology. He is now working on optimal thrust development in oscillating hydrofoils using active vorticity control at Korea Maritime University. His research interests are also measurement technique of particle sizing in spay flow and In vivo PIV measurement of capillary blood flow.

Young-Ho Lee: He graduated from Department of Marine Engineering, Korea Maritime University (KMU) in 1980. He acquired his master degree of Marine Engineering from KMU in 1982. He received his Ph.D. degree of Mechanical Engineering from University of Tokyo in 1992. He has been working in Division of Mechanical and Information Engineering, KMU as a faculty member since 1980. His research interests are quantitative flow informatics by PIV (time-resolved 2-D, surface flow, volume 3-D, stereoscopic 3-D, web visualization and animation contents) and Computational Fluid Dynamics (CFD). Main applications are turbo-machinery and renewable energy sources such as wind turbine and micro-hydro turbine.